THESIS FOR THE DEGREE OF DOCTOR OF PHILOSOPHY
IN
THERMO AND FLUID DYNAMICS

Numerical modeling of air–fiber flows

JELENA ANDRIĆ

Department of Applied Mechanics

CHALMERS UNIVERSITY OF TECHNOLOGY

Göteborg, Sweden, 2014

Numerical modeling of air–fiber flows

JELENA ANDRIĆ

Department of Applied Mechanics
Chalmers University of Technology

Abstract

The dynamics of fiber suspensions are of great importance in applications such as the dry-forming process of pulp mats for use in hygiene products. In this forming process, fibers are transported in flowing air. The fibers interact with the fluid, and may interact with each other and interlock in flocs. The characteristics of the suspension structure are essential for the design and optimization of the forming process, and for improving the quality of the final products. Particularly, it is desired to achieve a uniform fiber distribution in the pulp mats. Thus, it is of high interest to develop tools, which can be used to perform comprehensive studies of the complex phenomenon of fiber suspension flows.

This work is concerned with numerical analysis of fiber suspensions, related to the mat-forming process. For that purpose, a particle-level fiber model has been implemented into an open source computational fluid dynamics (CFD) code. A fiber is modeled as a chain of rigid cylindrical segments. The segments interact with the flow through hydrodynamic drag forces, and may interact with each other through short-range attractive forces. The segments are tracked individually using Lagrangian particle tracking (LPT). The implemented model comprises two alternatives, the flexible and the rigid fiber model, respectively. The equations of motion of a flexible fiber represent the application of Euler's second laws for rigid body motion for the fiber segments. The flexible fiber model takes into account all the degrees of freedom necessary to realistically reproduce the fiber dynamics. Connectivity forces act between the adjacent fiber segments to ensure the fiber integrity. The rigid fiber model keeps the relative orientation between the segments fixed. The equations of motion are formulated for the fiber as a whole, while the hydrodynamic contributions are taken into account from the individual segments. The fiber inertia is taken into account in both alternatives of the model. The fiber model has been coupled with imposed flow fields, or with flow fields computed by the CFD solvers.

The behavior of the implemented model is compared with analytical and experimental results available in the literature. The simulation results show that the model correctly predicts the dynamics of isolated

rigid and flexible fibers in creeping shear flow.

The model is used to study the dynamics of flexible and rigid fibers in high Reynolds number flows and in geometries that are representative for the mat-forming process. The effects of fiber properties, such as fiber inertia and fiber length are analyzed.

Simulations are carried out to investigate the rheology of suspensions of flexible and curved fibers in creeping shear flow of a Newtonian fluid. The effects of fiber flexibility and fiber curvature on the specific viscosity and the normal stress differences are examined.

Finally, aggregation of rod-like fibers is investigated in a turbulent flow of an asymmetric planar diffuser. The influences of the average flow gradient, the fiber inertia and the turbulence dispersion on the aggregation rate are analyzed. The study identifies a darting fiber motion as a mechanism that significantly enhances fiber collisions and aggregation.

List of Publications

This thesis is based on the following appended papers:

I   J. Andrić; S. T. Fredriksson; S. B. Lindström; S. Sasic; H. Nilsson, A study of a flexible fiber model and its behavior in DNS of turbulent channel flow, *Acta Mech*, 224, 2359-2374, 2013.

II J. Andrić; S. B. Lindström; S. Sasic; H. Nilsson, Description and validation of a flexible fiber model, implemented in a general purpose CFD code, 8th *International Conference on Multiphase Flow*, ICMF 2013, Jeju, Korea, May 26-31, 2013.

III J. Andrić; S. B. Lindström; S. Sasic; H. Nilsson, A particle-level rigid fiber model for high-Reynolds number flow, implemented in a general-purpose CFD code, 8th *International Conference on Multiphase Flow*, ICMF 2013, Jeju, Korea, May 26-31, 2013.

IV J. Andrić; S. B. Lindström; S. Sasic; H. Nilsson, Rheological properties of dilute fiber suspensions of rigid and flexible fibers, *Submitted for journal publication*.

V   J. Andrić; S. B. Lindström; S. Sasic; H. Nilsson, Numerical investigation of fiber flocculation on the air flow of an asymmetric diffuser, *To appear in Proceedings of the ASME 2014 4th Joint US-European Fluids Engineering Division Summer Meeting and 12th International Conference on Nanochannels, Microchannels, and Minichannels* , FEDSM 2014, August 3-7, 2014, Chicago, Illinois, USA.

Division of work between authors

This work was supervised by Prof. Håkan Nilsson and co-supervised by Dr. Srdjan Sasic. Prof. Alf-Erik Almstedt was also involved as a co-supervisor for the first two years. Dr. Stefan B. Lindström (Linköping University) has acted as co-supervisor during the final two years of the

project, providing his expertise in fiber suspension rheology and multi-phase flow simulations at the particle level.

The respondent is the principal author of the appended papers. The respondent was responsible for the fiber code development, and its integration in the open source software. The work presented in the papers was extensively discussed with the co-authors.

I Fredriksson set up and validated the flow case. The respondent was responsible for the numerical set-up, simulations, and post-processing of the fiber–flow cases. Lindström contributed with the study of fiber translational motion. The respondent prepared the manuscript, and the co-authors contributed with discussions. The manuscript was reviewed by the co-authors.

II Mathematical and numerical aspects related to the implementation of the elastic bending and twisting torques were extensively discussed with Lindström. The respondent carried out the simulations and postprocessed the results. The manuscript was written by the respondent and reviewed by the co-authors.

III Nilsson set up and validated the diffuser flow case. The rigid fiber model was discussed with the co-authors. The respondent carried out fiber–flow simulations and postprocessed the results. The respondent was responsible for writing the manuscript. The manuscript was reviewed by the co-authors.

IV Lindström analytically derived the estimate for the dipole strength. The respondent was responsible for the numerical implementation of the method. The simulations and postprocessing of the results were carried out by the respondent. The respondent prepared the manuscript in close collaboration with the co-authors.

V The respondent was responsible for the numerical set-up and validation of the diffuser flow case. The fiber-flow simulations were carried out by the respondent. The results were extensively discussed with the co-authors. The respondent prepared the manuscript, and the co-authors contributed with comments.

Acknowledgments

I would like to express my gratitude to:

- Supervisor Prof. Håkan Nilsson and co-supervisors Dr. Srdjan Sasic and Prof. Alf-Erik Almstedt for all their help, guidance and support.

- Co-supervisor Dr. Stefan B. Lindström (Linköping University), for joining and closely following the project, for his guidance, and for sharing his knowledge and experience.

- Dr. Henrik Rusche (Wikki GmbH) and Prof. Hrvoje Jasak (Wikki Ltd. and FSB Zagreb) for their help during NUMAP–Foam Summer school (Zagreb, 2011).

- Dr. Djordje S. Čantrak and Prof. Milan Lečić (University of Belgrade) for the useful technical discussions.

- Prof. Lars Davidson for sharing his expertise during the paper revision process.

- Anders Östin and his colleagues (SCA Hygiene Products AB) for showing me the industrial facility in Falkenberg, and discussing the mat-forming process.

- Monica, Ulla and Blagica for their invaluable help with administrative issues.

- My colleagues and friends at the division for creating a very pleasant atmosphere.

- My family for their love and support.

Nomenclature

Latin Symbols

d_i	Diameter of fiber segment i	[m]
l_i	Length of fiber segment i	[m]
N	Number of segments in a fiber	[–]
m_i	Mass of fiber segment i	[kg]
m	Fiber mass	[kg]
$\boldsymbol{I}_i$	Inertia tensor of fiber segment i	[kg m^2]
$\boldsymbol{r}_i$	Position vector of the center of mass of fiber segment i	[m]
$\dot{\boldsymbol{r}}_i$	Translational velocity of fiber segment i	[ms^{-1}]
$\ddot{\boldsymbol{r}}_i$	Acceleration of fiber segment i	[ms^{-2}]
$\boldsymbol{\omega}_i$	Angular velocity of fiber segment i	[s^{-1}]
$\hat{\boldsymbol{z}}_i$	Unit orientation vector of fiber segment i	[–]
$\boldsymbol{F}_i^h$	Hydrodynamic drag force on fiber segment i	[N]
$\boldsymbol{F}_i^w$	Gravitational body force on fiber segment i	[N]
$\boldsymbol{g}$	Gravitational acceleration	[ms^{-2}]
$\boldsymbol{X}_i^h$	Connectivity force exerted by segment i on segment $i-1$	[N]
$\boldsymbol{T}_i^h$	Hydrodynamic torque on fiber segment i	[Nm]
$\boldsymbol{Y}_i^h$	Bending and twisting torques exerted by segment i on segment $i-1$	[Nm]
r_f	Fiber aspect ratio	[–]
r_e	Equivalent aspect ratio	[–]
E_y	Young's modulus of fiber material	[Nm^{-2}]
T	Orbit period	[s]
L	Fiber length	[m]
n	Fiber number density	[m^{-3}]
$\boldsymbol{s}'$	Dipole strength	[Nm]
$\boldsymbol{s}^*$	Dimensionless dipole strength	[–]
N_1^*	Dimensionless first normal stress difference	[–]
N_2^*	Dimensionless second normal stress difference	[–]
F	Floc species	[–]

Greek Symbols

δ	Kronecker delta tensor	[–]
ϵ	Permutation tensor	[–]
ρ	Fluid density	[kgm^{-3}]
η	Fluid dynamic viscosity	[kgm^{-1}s^{-1}]
$\dot{\gamma}$	Characteristic shear rate of the flow	[s^{-1}]
η_{fib}	Fiber viscosity	[kgm^{-1}s^{-1}]
η_{sp}^{*}	Dimensionless specific viscosity	[–]
ϕ	Floc mass fraction	[–]
σ	Variance of fiber orientation	[–]

Contents

Chapter 1

Introduction

The dynamics of particles suspended in flowing fluid are of high importance in different processes in modern technology. In many of those suspensions nonspherical particles are present. Particularly, suspensions of fibers and fiber flocs are processed to produce paper products and fiber composites. Papermaking is a common industrial application in which fibers are transported in liquids. A number of studies that consider transport of fibers in water are found in the literature [1, 2]. Much less is known about the transport of pulp fibers in airflows. One example of such flows is dry-forming of pulp mats for use in hygiene products, such as diapers and sanitary napkins. In the dry-forming process, the fibers are introduced into airflow via a milling machine, and then transported through a divergent channel [3], see Fig.1.1. At the outlet of the channel, there is a rotating mat-forming wheel with a wire mesh. The fiber suspension is sucked through this moving form, and the fibers deposit on the mat-forming wheel to form the mat.

The suspension structure, whose development depends on fiber–flow interaction and fiber–fiber contacts, significantly influences the properties of the final products. In this dry-forming process, it is crucial to reach a uniform fiber distribution in the forming head. Analyzing the dynamics of fiber suspensions is thus of great importance for design and optimization of the forming process, and for improving the product quality. The goal of this work is to numerically investigate air–fiber suspensions, with the dry-forming process of pulp mats as the intended application.

1.1 Background and previous work

Fiber suspensions represent a complex two-phase system, which has been the subject of various theoretical, experimental and numerical
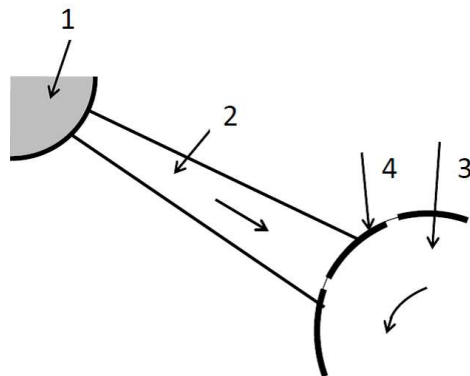
Figure 1.1: Mat-forming device; 1. milling machine, 2. transport channel, 3. mat-forming wheel, 4. mat form.

studies. The following sections give an overview of the relevant studies available in the literature.

1.1.1 Theoretical studies of fiber flows

Jeffery [4] derived the equations of motion of an isolated prolate spheroid in simple shear flow. The study showed that a spheroidal particle rotates in repeatable orbits around the vorticity axis, while neglecting particle and fluid inertia. Bretherton [5] discovered that all axisymmetric bodies experience similar orbiting behavior in simple shear flow. Cox [6] demonstrated that cylinders also exhibit Jeffery's orbits. The motion of isolated, inertialess, rigid, cylindrical fibers in creeping flow is thus relatively well understood.

On the other hand, in fiber suspensions there exist hydrodynamic and mechanical interactions among the fibers, which cause the fiber motion to differ from Jeffery's orbits [1]. The fiber suspensions can be classified into three different regimes, based on the fiber number density n, the fiber length L and the fiber diameter d: dilute regime ($nL^3 \ll 1$), semidilute regime ($nL^3 > 1$ and $nL^2d \ll 1$), and concentrated regime ($nL^2d > 1$). Batchelor [7] derived an expression for the average stress contribution from elongated rigid particles with a known orientation distribution. The study assumed that the particles are not interacting hydrodynamically with each other. Rahnama *et al.* [8] derived orientation distributions for semidilute suspensions, when the effect of hydrodynamic interactions between the particles are taken into account. Theoretical studies are thus limited to straight fibers and low fiber concentrations.

1.1.2 Experimental studies of fiber flows

There exist several experimental studies concerned with both individual fibers and fiber suspensions. Anczurowski and Mason [9] confirmed Jeffery's predictions for prolate spheroid motion in shear flow. Forgacs and Mason [10] studied the motion of isolated flexible fibers in creeping shear flow. They found that rigid fibers exhibit the same orbits as rigid cylinders, while the orbit periods of flexible fibers are significantly lower than those of straight, rigid fibers. Forgacs and Mason [10] identified five different regimes of fiber motion in creeping shear flow: rigid orbits, springy orbits, snake-like orbits, coiled orbits without entanglement and coiled orbits with entanglement. Their study showed that the dynamics of flexible fibers depend on the fiber stiffness, length, and the flow properties such as shear rate and fluid viscosity.

Ganani and Powell [11] reviewed experimental studies of rheology of concentrated suspensions of rod-like fibers in Newtonian and non-Newtonian fluids. Garner and Kerekes identified four different flow regimes for air–fiber suspensions with hardwood fibers, based on the distribution of fibers and their flocs: heterogeneous, flocculated, stratified and homogeneous. Stover *et al.* [12] measured the fiber orientation distribution in a Newtonian fluid with nearly linear flow gradient in semidilute regime. The results showed that for all investigated concentrations, the measured orientation distributions were similar to those predicted by Jeffery's theory [4]. Petrich *et al.* [13] investigated the relation between the microstructure and the rheological properties in the semiconcentrated fiber suspensions. Pettersson *et al.* [14] conducted a detailed study of the near-wall behavior in a pipe flow of fiber suspension using a laser Doppler anemometry (LDA) method. The study aimed at relating the LDA signal to fiber concentrations near the wall. The results showed that the width of the concentartion profile increased when the concentration decreased, and that the thickness of the dilution region was larger for the softwood fibers. Melander and Rasmuson [15] developed a particle image velocimetry (PIV) method to simultaneously measure the concentrations and the velocities of hardwood fibers suspended in the air. The developed method is feasible for air–fiber flows at low concentrations.

The phenomena related to fiber dynamics occur at the scales of a fiber length, and it is difficult to experimentally measure fiber shapes and deformations of flexible fibers [16], or the rheological properties of suspensions [17]. Therefore different numerical techniques have been developed to study the fiber dynamics.

1.1.3   Numerical modeling of fiber suspension flows

Two general numerical approaches have been developed to model fiber suspensions: the Eulerian–Eulerian approach, where both the particle phase and the fluid phase are treated as a continuum [18], and the Lagrangian–Eulerian approach, where the particles are treated as moving objects in the fluid medium [18]. Eulerian–Eulerian techniques are useful numerical tools to study fiber dynamics at industrial scales. The method has been used by several researchers. Ljus and Almstedt [19] used an Eulerian two-fluid model to investigate the transport of fibers in air in a mat-forming device. They carried out the simulations in two and three dimensions in a channel with and without a turbulence model for the gas phase. The study assumed that the fibers are rigid, single cylinders without angular rotation, and different drag coefficients were used for the parallel and perpendicular velocity components. The computed results for pressure and velocity were in good agreement with the experimental results in a similar channel.

Modeling different phenomena related to fiber suspension behavior often requires that an Eulerian–Eulerian model is combined with other modeling techniques, such as statistical methods [20]. The probability distribution of fiber positions and orientations is predicted using the convection-diffusion equation. In this approach, the mean flow convects the fiber positions and orientations, while the fluctuating component of the flow disperses the fibers. Olson *et al.* [21] proposed a one-dimensional headbox model, which employes the convection-diffusion equation to predict the fiber orientation distribution in a turbulent flow through a planar contraction. The computed fiber distributions were in agreement with experimental measurements. The study showed that the fiber orientation distribution depends on the dispersion coefficient and the contraction ratio. Krochak *et al.* [22] modeled fiber suspension flow in a tapered channel with low Reynolds number flow. They investigated the fiber reorientation, and the effect of the two-way coupling between the fibers and the flow. The study dealt with semidilute rigid fiber suspensions, and two different orientation states were considered at the inlet of the contraction. Krochak *et al.* [22] showed that the presence of the fibers significantly influences the velocity profiles independently of the initial fiber distribution. They argued that the fiber phase redirects the flow from the channels walls towards the middle of the channel and that the streamlines across the channel length become linear and closer to each other. They also found that the two-way coupling significantly influenced the fiber reorientation when a random inlet orientation was used. However, the majority of the Eulerian–Eulerian models assumes rigid fibers with the same properties and

negligible fiber–fiber contacts [22, 20]. These assumptions are not always valid for the actual industrial processes, which include fibers with various features and concentrated fiber suspensions.

In the Lagrangian–Eulerian approach, on the other hand, the particles are tracked individually using Lagrangian particle tracking (LPT). The method allows for detailed and accurate studies of particle-flow dynamics. For instance, in direct numerical simulations (DNS), the particle geometries are resolved at a high level of detail. Svenning *et al.* [23] used the immersed boundary method (IBM) to study the fiber suspension flow in the forming unit of a papermaking process under a laminar flow assumption. Wu and Aidun [16] applied the lattice-Boltzmann method (LBM) for direct simulation of flexible fibers in a Newtonian medium. Qi [24] also employed a direct simulation method, based on the lattice-Boltzmann equation, to simulate the motion of isolated flexible fibers. The study investigated the effects of flow inertia and fiber stiffness on fiber reorientation. These methods accurately predict fiber dynamics, but at a relatively high computational cost. Thus the microhydrodynamics approach, where many particles are combined into a multi-rigid-body systems [18, 25, 26], has been developed to study fiber suspensions.

1.1.4   Particle-level simulation technique

Several particle-level simulation techniques, which are using the microhydrodynamics approach, have been used for studying fiber suspension flows. The fibers are represented as multi-rigid-body systems of interconnected particles such as spheres, spheroids or cylinders. The equations of motion are solved for each individual particle, and the particle positions and orientations are evolved in time. These particle-level techniques permit for various fiber equilibrium shapes, and a finite fiber stiffness. The method makes it possible to account for various forces, such as hydrodynamic forces acting between the fibers and the flow, or interaction forces between the fibers [27]. Moreover, these techniques provide very detailed information about the suspension structures both in time and space, which cannot be easily accessed in experiments [20]. The particle-level methods are commonly employed to study fiber–flow interactions, fiber–fiber interactions, fiber flocculation, and how these phenomena influence the rheological properties of fiber suspensions.

Yamamoto and Matsuoka [28] developed a particle-level simulation technique to study the dynamics of rigid and flexible fibers in a prescribed flow field. They represented a fiber as a number of spheres,

lined up and connected to each neighboring sphere. The method was first applied to study the dynamics of isolated fibers in a simple shear flow. Their results were in qualitative agreement with experimental results for isolated fiber motion, reproducing the rigid, springy and snake-like regimes of fiber motion [29, 10]. This method was further extended to predict the viscosity of dilute suspensions of rod-like particles, and the behavior of concentrated fiber suspensions. Joung *et al.* [30, 31] proposed a similar model, where a fiber was modeled as a chain of spherical beads joined by connectors, and the method accounted for short- and long-range hydrodynamic interactions between these beads. They investigated the effect of fiber flexibility and curvature of rigid fibers on the suspension viscosity. Ross and Klingenberg [32] modeled a fiber as a chain of rigid prolate spheroids connected by ball and socket joints. The model included short-range hydrodynamic interactions between the fibers, and they investigated the transient behavior of the specific viscosity of the suspension. Their simulations for isolated fibers showed that the model can reproduce the known dynamics of both rigid and flexible fibers. These results demonstrated that fibers can be modeled as chains of rigid prolate spheroids. The possibility to model the fibers using fewer elongated bodies compared to many spherical particles significantly reduces computation time, and thus allows the study of fiber suspensions with a large number of slender fibers.

Schmid *et al.* [25] developed a particle-level simulation technique to study the flocculation of fibers in sheared suspensions. The fibers were modeled as chains of massless, rigid, cylindrical segments interacting with an imposed flow field through viscous drag forces and with other fibers through contact forces. The model did not account for particle inertia, hydrodynamic interactions, or the two-way coupling between the fibers and the flow. They investigated the influence of fiber flexibility, fiber equilibrium shapes, and frictional interparticle forces on flocculation and the rheological properties of suspension. Lindström and Uesaka [26] further developed the model of Schmid *et al.* [25] in an attempt to deal with the full complexity of fiber suspensions. The improved model accounts for the particle inertia and the hydrodynamic interaction between the fibers. They derived the approximation of the noncreeping interaction between fiber segment and the surrounding fluid, for larger segment Reynolds numbers, and took into account the two-way coupling between the fibers and the flow. Their simulations successfully reproduced different regimes of motion for threadlike particles ranging from rigid fiber motion to complicated orbiting behavior, including coiling with and without self-entanglement. Lindström and

Uesaka [33] predicted the rheological properties for fiber suspensions of various volume concentrations, where both hydrodynamic and mechanical fiber interactions were taken into account. They also investigated the effects of the fiber aspect ratio, the fiber concentration, and the inter-particle friction on the stress tensor of suspension and on fiber flocculation [17]. A particle-level model of Lindström and Uesaka [26] was used to simulate the paper sheet forming on roll-blade former [34] and a twin-wire former [35].

1.2 Thesis objectives

This thesis aims at developing a particle-level fiber model that can be applied to the dry-forming process of pulp mats. In this process, fibers suspended in air are made to flow through a filtration bed, forming the pulp mat. For the purpose of analyzing the complex dynamics of air–fiber flows, a computational code was developed and integrated in the OpenFOAM open source CFD software [36]. The implemented particle-level model is based on those initially proposed by Schmid et al. [25] and further developed by Lindström and Uesaka [26]. The OpenFOAM software represents a suitable platform for integrating numerical code, and provides several different CFD solvers for the flow field.

The focus of this work is on fundamental studies of air–fiber flows. The obtained results can be used for developing and validating the Eulerian–Eulerian models that are applicable on industrial scales. The results can also provide information useful for characterizing mechanical fiber properties that are difficult to access experimentally.

The main objectives of this thesis work can be summarized as follows:

- Validate the implemented model using theoretical and experimental studies of the motion of isolated fibers in creeping shear flow.

- Investigate the rheology of sheared fiber suspensions with a Newtonian fluid medium. There are very few studies concerned with realistic fiber properties, such as fiber deformability or different equilibrium shape. The impacts of these fiber properties on suspension rheology have not been completely understood. The aim of this study is to accurately predict the effects of fiber flexibility and fiber shape on the rheological properties of the suspension.

- Apply the fiber model to analyze the dynamics of flexible and rigid fibers in geometries and flow conditions representative for

the dry-forming process. The focus here is on analyzing translational fiber motion and fiber reorientation, and how these depend on the fiber properties, such as fiber inertia or fiber length.

- Address the phenomenon of fiber flocculation that is rarely mentioned in the literature. The focus is on identifying the mechanisms that govern flocculation in rod-like fiber suspensions in a turbulent flow field.

Chapter 2

Methodology

2.1 Fiber model

The particle-level fiber model comprises two alternatives: flexible and rigid. The fiber geometry is based on the concept of rigid cylindrical segments connected by ball and socket joints [25, 26]. In the flexible fiber model, the segments rotate and twist around the joints, replicating the fiber bending and twisting deformations, while the total fiber length remains constant. In the rigid fiber model, the relative orientation between the adjacent segments remains fixed, and the segments form a single rigid body.

In this section the fiber geometry is described, and the governing equations for both flexible and rigid fiber model are presented.

2.1.1 Fiber geometry

A fiber is modeled as a chain of N rigid cylindrical segments [25, 26], see Fig. 2.1. The segments are indexed $i \in [1, N]$, and their locations are specified with respect to a global Cartesian coordinate system Γ. The axes of the global coordinate system are defined by the base vectors $\{e_1, e_2, e_3\}$, and the origin is denoted by O. A single fiber segment has a diameter d_i, a length l_i, a start point P_i, and a unit vector $\hat{z}_i$, which is aligned with the segment. For each fiber segment, the position vector $r_i = \overrightarrow{OP_i} + l_i\hat{z}_i/2$ points out the center of mass of the fiber segment.

To model the fiber flexibility, the fiber equilibrium shape needs to be included in the geometry description. For this purpose, a local coordinate system Γ_i is associated with each fiber segment. The local coordinate system is defined by the orthonormal set $\{\hat{x}_i, \hat{y}_i, \hat{z}_i\}$ and its origin is P_i, which is the start point of segment i. The fiber equilibrium shape is defined by fixing a coordinate system $\{\hat{x}_i, \hat{y}_i, \hat{z}_i\}$ on each

segment i, and an equilibrium coordinate system $\{\hat{x}_i^{eq}, \hat{y}_i^{eq}, \hat{z}_i^{eq}\}$ for each segment i on the preceding segment $i - 1$. For a given local coordinate system Γ_{i-1} for segment $i - 1$, the angles ϕ_i and θ_i of twist and bend, respectively can be determined so that coordinate system Γ_i^{eq} can be calculated from Γ_{i-1}. The bending and twising torques act to restore the fiber equilibrium shape.
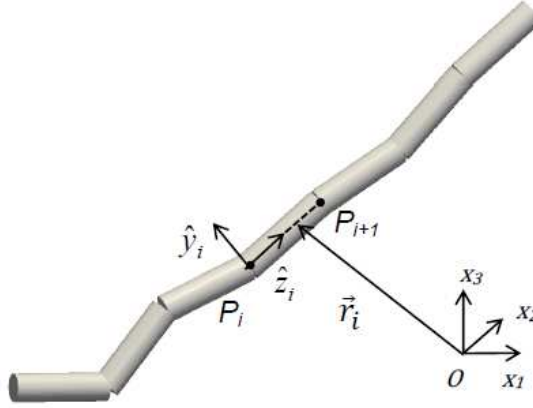

Figure 2.1: Fiber geometry definitions.

2.1.2   Flexible fiber equations of motion

The equations of motion of a flexible fiber represent the direct application of Euler's laws of rigid body motion for each fiber segment i [26, 25]. The rate of change of linear momentum of fiber segment i is the sum of all forces that act on the segment, i.e.

$$m_i \ddot{\boldsymbol{r}}_i = \boldsymbol{F}_i^h + \boldsymbol{X}_{i+1} - \boldsymbol{X}_i \tag{2.1}$$

Here, m_i is the mass of segment i, $\boldsymbol{F}_i^h$ is the hydrodynamic force acting on segment i, and $\boldsymbol{X}_i$ is the connectivity force exerted on segment $i - 1$ by segment i.

The rate of change of angular momentum about the center of gravity of the segment equals the sum of the moments of the external forces about that point, i.e.

$$\frac{\partial (\boldsymbol{I}_i \cdot \boldsymbol{\omega}_i)}{\partial t} = \boldsymbol{T}_i^h + \boldsymbol{Y}_{i+1} - \boldsymbol{Y}_i + \frac{l_i}{2} \hat{\boldsymbol{z}}_i \times \boldsymbol{X}_{i+1} + \left(\frac{-l_i}{2} \hat{\boldsymbol{z}}_i \right) \times (-\boldsymbol{X}_i) \tag{2.2}$$

where $\boldsymbol{I}_i$ is the tensor of inertia of segment i with respect to the global coordinate system Γ, $\boldsymbol{\omega}_i$ is is the angular velocity of segment i, $\boldsymbol{T}_i^h$ is
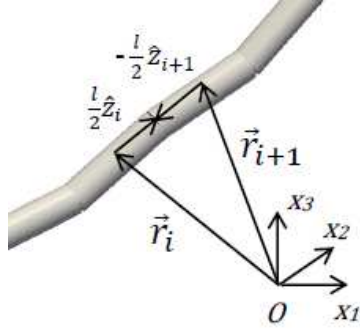
Figure 2.2: Kinematic relation between adjacent fiber segments.

the hydrodynamic torque acting on segment i, and $\boldsymbol{Y}_i$ is the sum of the bending and twisting torques exerted on segment $i-1$ by segment i.

The connectivity constraint represents a kinematic relation between the adjacent fiber segments, see Fig. 2.2. This constraint requires that the end-points of adjacent fiber segments coincide, i.e.

$$\boldsymbol{r}_i + \frac{l_i}{2}\hat{\boldsymbol{z}}_i = \boldsymbol{r}_{i+1} - \frac{l_{i+1}}{2}\hat{\boldsymbol{z}}_{i+1} \qquad (2.3)$$

The connectivity equation is then obtained by taking the time derivative of Eq. 2.3, i.e.

$$\dot{\boldsymbol{r}}_{i+1} - \dot{\boldsymbol{r}}_i = \frac{l_i}{2}\boldsymbol{\omega}_i \times \hat{\boldsymbol{z}}_i + \frac{l_{i+1}}{2}\boldsymbol{\omega}_{i+1} \times \hat{\boldsymbol{z}}_{i+1} \qquad (2.4)$$

Equations (2.1), (2.2) and (2.3) form the system of equations that can be solved for the unknown segment velocities and angular velocities. Those are used to evolve the segment positions and orientations. The hydrodynamic forces and torques exerted by the fluid on the fiber segments, the discretized equations of motion, and numerical algorithms to solve these equations were discussed in detail in Papers I and II.

2.1.3   Rigid fiber equations of motion

The equations of motions of a rigid fiber are defined for the center of mass of the fiber, taking into account the hydrodynamic forces exerted by the fluid on the fiber segments. The linear momentum equation of a fiber is then given by

$$m_i \ddot{\boldsymbol{r}}_G = \sum_i^N \{ \boldsymbol{F}_i^h + \boldsymbol{F}_i^w \}. \qquad (2.5)$$

11

Here, $\boldsymbol{r}_G$ is the center of mass of the fiber, and $\boldsymbol{F}_i^w = m_i \boldsymbol{g}$ is the gravitational body force.

The angular momentum equation of a fiber reads

$$\boldsymbol{I}_G \cdot \dot{\boldsymbol{\omega}} + \boldsymbol{\omega} \times (\boldsymbol{I}_G \cdot \boldsymbol{\omega}) = \sum_i^N \{\boldsymbol{T}_i^h + \boldsymbol{r}_{G_i} \times (\boldsymbol{F}_i^h + \boldsymbol{F}_i^w)\}, \qquad (2.6)$$

where $\boldsymbol{\omega}$ is the angular velocity of the fiber, $\boldsymbol{I}_G$ is the fiber inertia tensor with respect to its center of mass and the global reference frame Γ, and $\boldsymbol{r}_{G_i} = \boldsymbol{r}_i - \boldsymbol{r}_G$. Equations (2.5) and (2.6) form the system of equations that can be solved for the linear and angular velocities of a fiber. The linear velocities of the fiber segments are then computed, and the fiber positions and orientations are updated. The discretized governing equations, the numerical schemes to solve these equations, and the time step constraints were discussed in detail in Paper III.

2.2 Flow representation

The representation of the flow field is dependent on the type of the study that is carried out.

A prescribed creeping shear flow with the one-way coupling between the fibers and the flow was used for the purpose of validating the implemented fiber model. An analytical expression was used to describe the fluid motion, i.e.

$$\boldsymbol{v}(\boldsymbol{x}) = (\dot{\gamma}y, 0, 0). \qquad (2.7)$$

Here, $\boldsymbol{v}$ is the flow velocity, and $\dot{\gamma}$ is the shear rate.

A creeping shear flow, predicted by the CFD solver, was used to include the two-way coupling between the fibers and the fluid flow. The three-dimensional incompressible Navier–Stokes equations were employed to describe the fluid motion, i.e.

$$\nabla \cdot \boldsymbol{v} = 0, \qquad (2.8)$$

$$\frac{\partial \boldsymbol{v}}{\partial t} + \boldsymbol{v} \cdot \nabla \boldsymbol{v} - \frac{\eta}{\rho} \nabla^2 \boldsymbol{v} = -\frac{1}{\rho} \nabla p, \qquad (2.9)$$

where ρ is the density of the fluid, η is its dynamic viscosity, and p is the static pressure.

The dynamics of fibers were analyzed in turbulent flow fields. Equations 2.8 and 2.9 were solved using either DNS, or standard eddy-viscosity turbulence models, where the dynamic viscosity contains the

contributions from turbulence. The simulation methods were chosen to correctly capture the physics of the system, while allowing for reasonable computational times.

Chapter 3

Specific results

3.1 Motion of isolated fibers in shear flow

The motion of isolated fibers in shear flow is studied in Papers II, III and IV, with the purpose of validating the implementations of the fiber model.

3.1.1 Rigid fibers

The motion of isolated, straight, rigid fibers in creeping shear flow is relatively well understood through several theoretical studies. Jeffery [4] showed that a prolate spheroid undergoes periodic motion and spends most of time aligned with the flow direction while orbiting. Bretherton [5] later demonstrated that circular cylinders experience similar orbiting behavior in simple shear flow. Cox [6] derived a semi-empirical expression for the orbit period of a circular cylinder, which uses an equivalent aspect ratio instead of the actual spheroid aspect ratio.

Simulations of isolated rigid fibers were carried out in creeping shear flow using both the flexible fiber model, with stiff fiber properties, and the rigid fiber model. The simulated orbit period of the rigid fiber was compared with the one computed using Jeffery's equation [4] in conjunction with Cox's formula [6] for an equivalent aspect ratio. The simulated orbit period in a prescribed shear flow with the one-way coupling between the fiber and the fluid phase was overpredicted by $10 - 20\%$, see Paper II for the flexible fiber model and Paper III for the rigid fiber model. The overprediction of the orbit period was believed to be due to the one-way coupling between the fibers and the flow, as suggested by Lindström and Uesaka [26]. The analysis of the orbit period was also conducted in a simultaneously predicted shear flow with the

15

two-way coupling between the fibers and the fluid flow. The computed orbit period and the orbit period obtained from the theoretical prediction were compared for different fiber aspect ratios, r_f. The discrepancy increased with fiber aspect ratio from 5% for a fiber with $r_f = 15$ to 12% for a fiber with $r_f = 55$. It was concluded that the discrepancy remained despite accounting for the two-way coupling.

3.1.2   Flexible fibers

Forgacs and Mason [29] theoretically studied the flexible fiber behavior in creeping shear flow. They derived a critical value of $\dot{\gamma}\eta$ at which the axial compression due to hydrodynamic forces causes a fiber to buckle. A cylindrical fiber, orbiting in the flow-gradient plane, ie expected to buckle when a dimensionless bending ratio [25]

$$BR \equiv \frac{E_y[\ln(2r_e) - 1.50]}{2\eta\dot{\gamma}r_f^4},$$ (3.1)

is less than unity. Here, E_y is the Young's modulus of the fiber material, and r_e is an equivalent fiber aspect ratio. The experimental studies of Forgacs and Mason [10] identified five different regimes for fiber motion in creeping shear flow: rigid orbits, springy orbits, snake-like orbits, coiled orbits without entanglement, and coiled orbits with entanglement. Schmid *et al.* [25] employed a particle-level model to simulate the motion of isolated fibers, while varying fiber stiffness. They showed that intrinsically straight fibers bend into the symmetric S-shapes. Moreover, the study demonstrated that fibers with initial small radius of curvature bend into the experimentally observed C-shapes [10]. Both the study of Schmid *et al.* [25] and the study of Lindström and Uesaka [26] qualitatively predicted the rigid, springy and snake-like regime of motion.

The simulated orbits in Paper I were in qualitative agreement with those observed in experimental studies for the rigid, springy and snake-like orbit type, respectively, see Fig. 3.1. Similarly, simulations were carried out in Paper IV for intrinsically straight fibers with moderate bending ratio. The study considered fibers with aspect ratio $r_f = 55$, consisting of 11 segments. The resulting shapes were in qualitative agreement with those observed by Schmid *et al.* [25], who used 10 segments to model fibers with $r_f = 50$, see Fig. 3.2. The buckling transition occurred at $BR \approx 0.03$, a slightly lower value than $BR \approx 0.1$, which was observed in the work of Schmid *et al.* [25]. This is most likely the consequence of the two-way coupling between the fibers and the fluid flow, considered in Paper IV.

The main conclusions from the simulation results are that the flexible fiber model predicts the dynamics of both rigid and flexible fibers, and that the rigid fiber model predicts the dynamics of rigid rod-like fibers, in creeping shear flows.
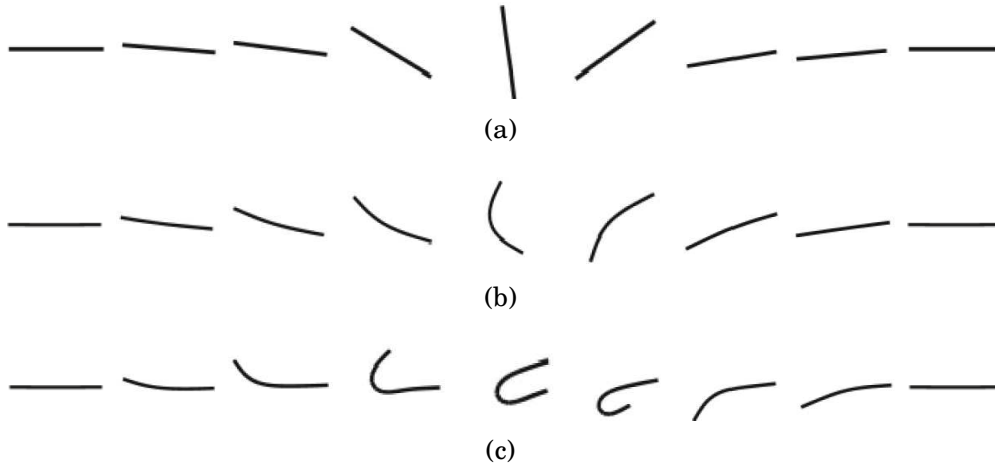

(a)

(b)

(c)

Figure 3.1: Time-series of simulation results for fiber shape development in simple shear flow during half a period of revolution. Each case corresponds to an actual experiment by Forgacs and Mason [10]. Three different orbit types are observed: a) rigid, b) springy and c) snake-like. The fiber diameters are exaggerated for the purpose of visualization.

3.2   Fiber suspensions in shear flow

The rheology of fiber suspensions was investigated in Paper IV. The work was concerned with dilute suspensions of flexible and curved fibers. A novel method for computing the fiber contribution to the deviatoric stress was proposed to account for the fiber flexibility and different fiber equilibrium shapes.

3.2.1   Fiber contribution to deviatoric stress

The theoretical expression of Batchelor [7] for the contribution of a fiber to the deviatoric stresses applies to dilute suspensions of straight, slender, rigid fibers in creeping shear flow. To the knowledge of the author, there is no theoretical study that describes the contribution of flexible or curved fibers to the deviatoric stresses in a similar manner.

Several authors numerically studied the effects of fiber stiffness and fiber shapes on suspension rheology. Schmid *et al.* [25] found that in-
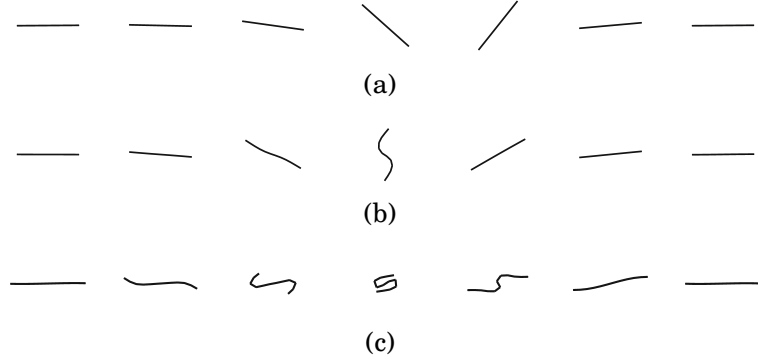
Figure 3.2: Time-series of simulation results for fiber shape development during half a period of revolution ($r_f = 55$, $N = 11$). Each case corresponds to different fiber bending ratio a) $BR = 1$, b) $BR = 0.02$, c) $BR = 0.0016$. The fiber diameters are exaggerated for the purpose of visualization.

trinsically straight flexible fibers produce higher values of the first normal stress difference than rigid fibers. Their study did not contain results about the specific viscosity. Joung *et al.* [30, 31] investigated the effects of fiber flexibility and fiber curvature on the specific viscosity in concentrated fiber suspensions. Their study showed that the specific viscosity increases with fiber flexibility. The aforementioned numerical studies used Batchelor's theory to compute the deviatoric stresses of flexible and curved fiber suspensions.

The novel method, proposed in Paper IV, considers the hydrodynamic forces and torques acting on the fiber segments as localized tractions. Starting from the equation for dipole strength of a slender cylinder [37], a dipole strength s' from a single fiber was obtained as

$$s' = \sum_{i=1}^{N} [\boldsymbol{F}_i^h \boldsymbol{r}_i - \frac{1}{2}\boldsymbol{\epsilon} \cdot \boldsymbol{T}_i^h - \frac{1}{3}(\boldsymbol{r}_i \cdot \boldsymbol{F}_i^h)\boldsymbol{\delta}], \qquad (3.2)$$

where $\boldsymbol{\delta}$ and $\boldsymbol{\epsilon}$ are the unit and the permutation tensor, respectively. A detailed derivation of Eq. 3.2 is presented in Paper IV.[1]

A dimensionless dipole strength was introduced as

$$s^* = \frac{n}{\eta_{fib}\dot{\gamma}}s'. \qquad (3.3)$$

---

[1]The results presented in Fig. 3.3 and Paper IV are obtained with an implementation error using the $+$ sign in front of $\frac{1}{2}\boldsymbol{\epsilon} \cdot \boldsymbol{T}_i^h$ term. The simulations using the correct expression for s' were carried out for rigid fiber with $BR = 5$ and $r_f = 55$. The obtained results did not differ from those presented in Paper IV for the corresponding case, i.e. this term did not affect the simulation results.

Here, n is the fiber number density and η_{fib} is the fiber viscosity [7] given by

$$\eta_{fib} = \frac{\pi n L^3 \eta}{6 \ln(2r_f)} f(\epsilon),$$ (3.4)

where L is the fiber length, and $f(\epsilon)$ is a correction factor for finite aspect ratio and cylindrical shape. The proposed estimate for the dipole strength was in good agreement with the dipole strength computed using Batchelor's theoretical expressions in conjunction with the computed fiber orientation for rigid fibers with $BR = 5$ and two different fiber aspect ratios $r_f = 55$ and $r_f = 35$, respectively.

Ergodicity was assumed, i.e. the ensemble average of the deviatoric stress from multiple fibers is assumed identical to the time average from a single fiber, yielding

$$\langle \boldsymbol{s} \rangle = \frac{1}{T} \int_t^{t+T} \boldsymbol{s}'(t) dt,$$ (3.5)

where T is the orbit period, and $\boldsymbol{s}'$ is the dipole strength from one particular fiber. Using Eq. 3.5, the specific viscosity and the dimensionless first and second normal stress differences were computed as

$$\eta_{sp}^* = \langle s_{21}^* \rangle,$$ (3.6)
$$N_1^* = \langle s_{11}^* - s_{22}^* \rangle,$$ (3.7)
$$N_2^* = \langle s_{22}^* - s_{33}^* \rangle,$$ (3.8)

for the duration of five half-periods of Jeffery's orbits.

The effects of the fiber flexibility and the fiber curvature on the specific viscosity and the normal stress differences were investigated. The results were discussed in detail in Paper IV. The most important observation is related to the specific viscosity of the suspension, and it is thus reviewed in the next subsection.

3.2.2 Effects of fiber flexibility on suspension viscosity

The effects of fiber flexibility on the suspension viscosity were investigated for fibers with a straight equilibrium shape and moderate values of bending ratio BR. These ideally straight fibers buckle into an S-shape, as it was previously discussed in Sect. 3.1. Figure 3.3 illustrates the relation between the specific viscosity and fiber bending ratio, BR. For stiff fibers, i.e. for the higher BR values, the results obtained using Batchelor's theoretical expression in connection with the computed
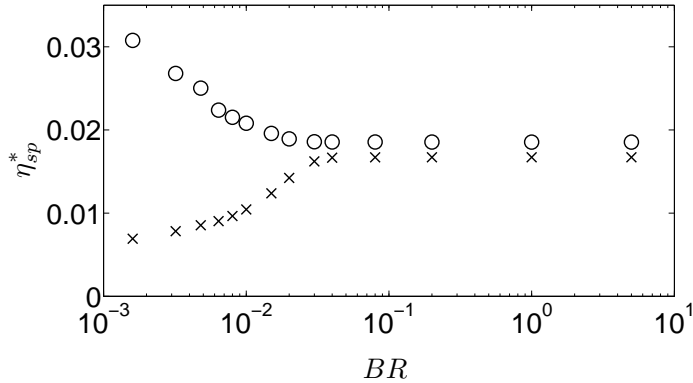
Figure 3.3: Relation between fiber bending ratio *BR* and specific viscosity for $r_f = 35$. The ×-symbols are the simulation results; marker ○ is Batchelor's theoretical expression.

fiber orientation are in good agreement with the results computed using the proposed direct method. When fiber flexibility increases, the specific viscosity computed using Batchelor's theoretical prediction increases, which has already been observed by Joung *et al.* [31] and Wu and Aidun [16]. The present work argues that their results do not represent the true physics since flexible fibers are beyond the validity range of Batchelor's theory. When applying the direct method for computing the deviatoric stresses, there is a sharp knee in the curvature at which point the specific viscosity decreases. The ability of the fiber to buckle reduces the fiber-induced flow gradients, which decrease the viscous dissipation caused by the fiber, and thus the specific viscosity of the suspension. This observation highlights the necessity to properly account for a flexible fiber contribution to the deviatoric stress.

3.3 Fiber suspensions in realistic flow fields

The dynamics of air–fiber suspensions were analyzed in geometries and flow conditions, which are reasonably representative for the actual dry-forming of pulp mats. The turbulent flow in a plane channel was considered in Paper I. The fibers were inserted in the fully developed turbulent flow field, computed using the DNS technique. The fiber motion was simultaneously solved with the fluid flow field. The ERCOFTAC conical diffuser [38] with a turbulent Newtonian flow was used as the case in Paper III, while an asymmetric planar diffuser [39, 40] was used in Paper V. The standard $k - \epsilon$ and $k - \omega$ turbulence models were

employed to model the turbulence in Papers III and V, respectively. The flow conditions accounted for high Reynolds number flows and finite Reynolds number fiber–flow interactions [1]. The parameters of the fibers, such as diameter, length, and density were consistent with those of hardwood fibers, which are typically used in the production of pulp mats.

The air-fiber dynamics in the mat forming process govern fiber reorientation and fiber flocculation, which significantly influence the quality of the final products, as discussed in Chap. 1.

3.3.1   Fiber alignment

The alignment in the flow direction of flexible and rigid fibers was analyzed in a turbulent flow field in Papers I and III, respectively. The fiber orientation is well understood only for suspensions of rigid, straight fibers in creeping shear flows. Stover *et al.* [12] showed that fibers in semidilute suspensions rotate around the vorticity axis, and spend most of the time aligned with the flow–gradient plane similarly to Jeffery's orbits [4]. Nevertheless, several studies focused on identifying different parameters that influence fiber orientation distribution [21, 22]. The process of fiber alignment is generally known to be governed either by the gradient of the average flow field, or by the turbulence fluctuations.

The present study required to define the fiber orientation for nonstraight fibers. The orientation of a fiber with N segments was here defined as

$$\hat{\boldsymbol{z}} = \frac{\boldsymbol{z}}{|\boldsymbol{z}|}, \quad \boldsymbol{z} = \sum_{i=1}^{N} \hat{\boldsymbol{z}}_i,$$

where the summation is over the fiber segments. For a rigid, straight fiber, all the segments have the same orientation, which is the orientation of the fiber. The alignment of the fiber with the flow direction was defined by

$$z_1 = \hat{\boldsymbol{z}} \cdot \hat{\boldsymbol{e}}_1, \quad -1 \leq z \leq 1,$$

where $\hat{\boldsymbol{e}}_1$ is the unit vector pointing in the flow direction. The absolute value $|z_1|$ was used to quantify the orientation to account for the ambiguity in the enumeration of fiber segments. Moreover, the variance of the orientation was defined as

$$\sigma_{\hat{\boldsymbol{z}}}^2 = \frac{1}{N-1} \sum_{i=1}^{N} |\hat{\boldsymbol{z}}_i - \hat{\boldsymbol{z}}|^2.$$

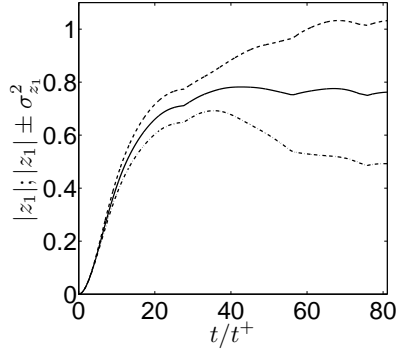The variance is zero for straight fibers and increases as the fiber shape becomes coiled.

Figure 3.4: The alignment of fibers initially closest to the walls. (a) Solid curve: ensemble average of $|z|$; dashed curve:$|z| + \sigma_{z_1}^2$; dash-dotted curve:$|z| - \sigma_{z_1}^2$.

The development of the ensemble average for $|z_1|$ was investigated for flexible fibers in Paper I. The initially straight and vertical fibers were distributed at the channel inlet at different distances from the walls. The ensemble average $|z_1|$ of the fibers initially closest to the walls are plotted in Fig. 3.4. Two characteristic time-scales are observed. The first time-scale of the initial ramp ≈ 13 is in the order of the inverse shear rate as predicted by Jeffery [4] for stiff fibers in a simple shear flow. The signed orientation shown in Fig. 3.5(a) reveals that fibers mainly rotate with the flow vorticity, indicating that the alignment is governed by the average flow gradients. The second time-scale is associated with randomization of the orientation of the individual fibers, and it is not consistent with the half-period of Jeffery's orbits ≈ 3378 for stiff fibers. The plot of variance in Fig. 3.5(b) shows that the fibers evolve into complex geometrical configurations in a turbulent flow field. The simulation time was not sufficiently long to evaluate the steady-state characteristics of these coiled configurations.

The alignment of rigid, straight fibers was investigated in Paper III. The study showed that the orientation exhibits an initial ramp in order of the inverse shear rate, i.e. that the fiber reorientation is driven by the average flow gradients.

Both studies investigated the effects of fiber properties, such as fiber length and fiber density, on the fiber reorientation. It was found that the orientation change in the initial phase is slower for the heavier particles. The inertia of the fibers thus influenced the time-scales of fiber reorientation. When the segment length was varied, no significant effect on fiber reorientation was observed.
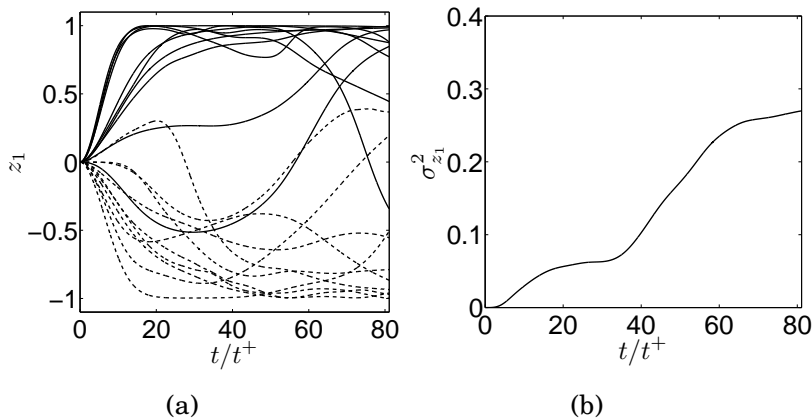
(a)   (b)

Figure 3.5: (a) Orientational component z_1 for the individual fibers. (b) Variance.

3.3.2 Fiber flocculation

The phenomenon of fiber flocculation was addressed in Paper V. The study was concerned with dilute suspensions of rigid, straight fibers in an asymmetric planar diffuser [39, 40]. A steady-state flow model was used for the diffuser, and the resulting flow field was used for integrating the fiber motion using the rigid fiber model. A stochastic model was employed to capture the turbulent fiber dispersion [41]. The fibers were assumed to interact through short-range attractive forces that cause them to interlock in flocs each time fiber–fiber contacts occur. Both fiber positions and fiber orientations were initially uniformly randomized. Fibers that crossed a specific outlet plane re-entered the diffuser at the inlet plane, and the total number of fibers remained constant in the diffuser. The simulations were carried out until a fully developed fiber–flow solution was reached.

Different floc species F_k were identified, based on the number of fibers, k, that they contain. The computational domain was divided in equally thick control volumes (CV) along the flow direction, and the mass fraction ϕ_2 of species F_2 was computed for each CV. The development of the mass fraction, ϕ_2, of the F_2 species is shown in Fig. 3.6. The flocculation rate decreases in the region that corresponds to the inflow channel section and the beginning of the diffuser section. Then, an elevation in the flocculation rate is observed in the diffuser section. Namely, the average flow velocities decrease through the diffuser section. The velocity gradient in the flow direction and the inertia of the fibers lead to a velocity difference between the fibers and the flow. This velocity difference in combination with the oriented dynamic resistance
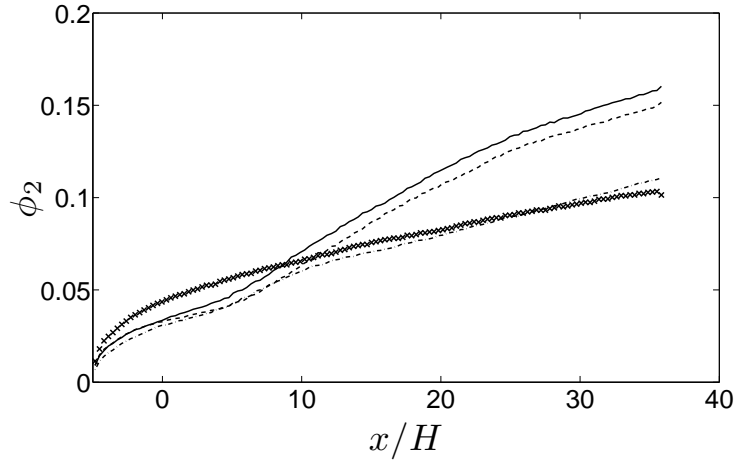
23

Figure 3.6: Mass fraction of floc species F_2 along the diffuser. Solid curve: with dispersion model; Dashed curve: without dispersion model; Dash-dotted curve: low-inertia fiber with dispersion model. Marker $\times$: straight channel flow with dispersion model.

tensors of the fibers [26] lead to darting fiber motion, which significantly increases the contacts between the fibers. The darting fiber motion is thus believed to cause the elevation in the flocculation rate, and to contribute to sustaining the flocculation rate downstream the diffuser. Further, when the random walk model for turbulent dispersion is switched off, the curve of the mass fraction ϕ_2 has the same trend as that with the dispersion model, but the values are slightly lower. The turbulence dispersion thus influence the rate at which fiber flocculate. But more importantly, the effect of the darting motion is much larger. Moreover, in the inflow region the curves of ϕ_2 obtained with and without the dispersion model overlap each other, most likely due to the inbalance of fiber kinematics at the inlet.

The influence of the fiber inertia on the flocculation rate was analyzed by decreasing the fiber density by a factor five. The result shows that the flocculation rate again decreases in the inflow channel region and the beginning of the diffuser section. The darting fiber motion in this section is reduced, and the initial flocculation rate is lower compared to the case with large-inertia fibers. The flocculation rate then increases in the first half of the diffuser section, but contrary to the case with larger-inertia fibers, remains nearly constant in the second half of the diffuser and in the outflow section. The inertia of the fibers clearly influences the flocculation rate in the diffuser.

Further, to investigate the effect of the average flow gradients on

24

the flocculation rate, the same analysis was carried out for a straight channel geometry with the same height as the inlet section of the diffuser geometry. The results are included in Fig. 3.6 for comparison. The flocculation rate first decreases and then remains nearly constant throughout the channel. The flocculation in the channel is governed by turbulence dispersion, and the effects of the inlet. It should be noted that the total number of fibers is the same in all the simulations. This gives a higher fiber number density in the channel case, which explains the higher level of flocculation in that case.

These observations demonstrate that the turbulence dispersion and the darting motion of the fibers, triggered by the average flow gradients and the fiber inertia, are the mechanisms of the flocculation in suspensions of rigid, straight fibers.

Chapter 4

Summary of papers

This chapter provides a short summary of the work that has been presented in the papers, on which this thesis is based.

4.1 Paper I

Paper I provides a detailed description of the implemented particle-level fully flexible fiber model. A fiber is modeled as a chain of rigid cylindrical segments [25, 26]. The equations of motion of a fiber account for the fiber inertia, the hydrodynamic forces and torques exerted by the fluid on the fiber segments, and the connectivity forces that act among the adjacent fiber segments to ensure fiber integrity. Bending and twisting torques are neglected, as well as fiber–fiber and fiber–wall interactions.

The dynamics of isolated fully flexible fibers are analyzed in a turbulent channel flow. A DNS of the three-dimensional incompressible Navier–Stokes equations is used to predict the fluid motion. A one-way coupling between the fibers and the fluid is considered.

The translational motion of the fibers is investigated using the mean square displacement (MSD) of their trajectories. It is found that the fibers are superdiffusive at the investigated time scales, and that the fiber motion is mainly governed by the flow fluctuations.

The reorientation of fibers has been studied. Two characteristic time-scales are observed. The first time-scale of the initial ramp is in order of the inverse shear rate, as predicted by Jeffery [4] for the fibers aligned in the shear gradient direction. The second time scale is inconsistent with the half-period of Jeffery's orbits for the stiff fibers. This reorientation is not understood as an alignment, but as a randomization of the orientation of the individual segments. The initially straight fibers evolve into complex geometrical configurations in the turbulent

flow field.

The influence of the fiber properties is also investigated. It is found that the fiber inertia affects the time-scales of the fiber reorientation, while the fiber length does not have any significant effect on the fiber motion.

4.2   Paper II

The fully flexible fiber model, implemented in Paper I, is extended to account for the elastic bending and twisting torques to model the finite fiber stiffness. The purpose of Paper II is to validate the complete fiber model for the motion of isolated fibers in prescribed creeping shear flow. The simulations were carried out in a box-shape computational domain with a prescribed simple shear flow.

For a fiber with properties that make it stiff and straight, the computed period of rotation is shown to be in good agreement with the one computed using Jeffery's equation [4] in conjunction with Cox's [6] formula for an equivalent spheroid aspect ratio. Further, qualitative comparisons are made for flexible fibers corresponding to three experimental instances [10], which belong to the rigid, springy and snake-like regime, respectively. The numerical results qualitatively agree with the experimental observations for each orbit type. The validation thus demonstrates that the fiber model successfully reproduces the known dynamics of rigid and flexible fibers.

4.3   Paper III

The focus of Paper III is on the dynamics of fibers in a realistic flow field, representing one stage in the actual dry-forming process. For that purpose, a rigid particle-level model is implemented. The fibers are modeled as chains of rigid cylindrical segments, and the fiber translational and rotational degrees of freedom are considered. The equations of motion account for the segment inertia, for the hydrodynamic forces and torques exerted by the fluid on the fiber segments, and for the gravitational body force acting on the fiber segments. Fiber–fiber and fiber–wall interactions are neglected. The implemented model is validated for the rotational motion of isolated fiber in a prescribed creeping shear flow.

The fiber model is applied to the swirling flow of the ERCOFTAC conical diffuser [38]. The incompressible Reynolds-averaged Navier-Stokes equations with the standard $k - \epsilon$ turbulence model are used

to predict the fluid motion. A one-way coupling between the phases is assumed. The reorientation of the fibers is investigated for different lengths and densities of the fibers.

It is found that the alignment of the fibers is mainly governed by the average flow gradients, and that the fiber inertia affects the time scales of fiber reorientation. The fiber length is found to have a negligible effect.

4.4   Paper IV

Paper IV investigates the rheology of sheared fiber suspensions with a Newtonian fluid. The work investigates the effects of fiber flexibility and fiber shape on the rheological properties of fiber suspensions. A novel method is proposed to compute the fiber contribution to the deviatoric stress of dilute, monodispersed fiber suspension, accounting for the fiber shape fluctuations. Particle-level simulations are carried out for isolated flexible fibers in creeping shear flow with the two-way coupling. Ergodicity is assumed and the deviatoric stress from an ensemble of fibers is replaced by a time average of a single fiber. Both the fiber model and the flow simulations are fully three-dimensional. However, the initial fiber configuration is coplanar with the flow–gradient plane. As a consequence, the fiber motion remains in this plane. This choice is made because of the existing theoretical and experimental studies, in which the fiber motion is considered in the flow–gradient plane.

The proposed method for computing the dipole strength of a single fiber is validated against Batchelor's theoretical prediction [7] for rigid, straight fibers. The non-zero dipole strength components computed using the proposed method are in good agreement with those obtained using Batchelor's theoretical expression in combination with the computed fiber orientation.

The study investigates the effects of the fiber flexibility and the fiber shape on the specific viscosity and the normal stress differences. It is found that the first and the second normal stress differences increase as fiber flexibility increases, which is in agreement with what has been observed before [25, 16, 30]. Both the first and second normal stress differences are shown to converge to zero for larger bending ratios, as predicted by Batchelor's theory for rigid, straight fibers together with a symmetric orientation distribution. Further, it is observed that the specific viscosity decreases as the fiber flexibility increases. This observation contradicts the previous results of Joung *et al.* [30] and Wu and Aidun [16], where Batchelor's theory [7] was applied to flexible fiber

suspensions. This finding highlights the necessity to correctly account for the shape fluctuations of flexible fibers while predicting their effects on the rheological properties of the suspension.

The effects of fiber equilibrium shape are analyzed using curved fibers with a high bending ratio $BR = 5$. A significant increase in the normal stress differences is observed as the fiber curvature is increased. The normal stress differences return to zero, as the fiber symmetry is restored. When the fiber shape is nearly straight, the normal stress differences converge to zero, which corresponds to Batchelor's theory. This is consistent with previous observations when the fiber flexibility is varied.

The predicted rheological properties of fiber suspensions can be used in the experimental characterization of fiber morphology and fiber mechanical properties. The stiffness of the elongated colloid and macromolecules can be found by varying the shear rate and identifying the crucial rate at which the first normal stress difference takes a finite value, or a distinct knee in the viscosity curve occurs.

4.5   Paper V

Paper V constitutes a step towards investigating the phenomena of fiber flocculation. The rigid particle-level fiber model, implemented in Paper III, is employed to study the flocculation in dilute suspension of rigid, straight fibers. An asymmetric planar diffuser [39, 40] is used as the flow case, representing an actual geometry in the dry-forming process. The fluid motion is predicted by the Reynolds-averaged Navier–Stokes equations with the standard low-Reynolds $k - \omega$ turbulence model. A stochastic model is employed to capture the fiber dispersion. A one-way coupling between the phases is assumed. The fibers are assumed to interact through short-range attractive forces, which cause them to interlock in flocs when fiber–fiber contacts occur.

The fibers are suspended in the steady-state flow of the diffuser, and their positions and orientations are uniformly randomized. Fibers that cross the specified outlet plane re-enter the diffuser at the specified inlet plane, keeping the total number of fibers constant in the diffuser. The contact model is employed at each time step to identify all fiber–fiber interactions. The simulations are run until a steady-state fiber flow solution is reached.

The development of floc mass fraction along the diffuser is investigated. The turbulent kinetic energy and the average flow gradient are analyzed to identify their effects on the flocculation. It is observed that the flocculation rate decreases in the inflow channel region and

the beginning of the diffuser section. Subsequently, an increase in the rate of flocculation is observed in the diffuser. A darting fiber motion is found to enhance the collisions between the fibers, and consequently the flocculation rate. The equivalent study in a straight channel confirmed the effects of the average flow gradients and fiber inertia on the development of the mass fraction curve.

The work thus argues that the turbulence dispersion and the darting motion of fibers, caused by the flow gradients, are the main mechanisms responsible for fiber flocculation in dilute rod-like fiber suspensions.

Chapter 5

Concluding remarks

A particle-level fiber model has been integrated in the OpenFOAM open source CFD software [36]. Each fiber is modeled as a chain of cylindrical segments [25, 26] that are tracked individually using Lagrangian particle tracking (LPT). The segments interact with the fluid flow through hydrodynamic drag forces, and may interact with each other through short-range attractive forces. The segment inertia is taken into account. The present work comprises two alternatives of the fiber model: flexible and rigid. The equations of motion of a flexible fiber represent the direct application of Euler's laws for each individual segment. These equations account for the connectivity forces and moments that ensure the fiber integrity. The elastic bending and twisting torques are taken into account in Papers II and IV, but not in Paper I. For the rigid fiber model, the relative angle between the orientation vectors of the adjacent segments is constant, so that the segments together form a single rigid body. The equations of motion are then formulated for the fiber as a whole, taking into account the hydrodynamic contributions from the individual segments.

The model is applied in imposed flow fields given by analytical expressions, and in flow fields predicted by the CFD solver. For the latter ones, the fluid motion is described by the incompressible Navier–Stokes equations in two and three dimensions. Both one- and two-way coupling between the fibers and the flow are considered.

The fiber model is validated against known theoretical and experimental results for the motion of isolated rigid and flexible fibers in creeping shear flow. The computed orbit periods for rigid, straight fibers are in good agreement with those obtained from Jeffery's equations for equivalent aspect ratios [4, 6]. The simulated orbits of flexible fibers are in qualitative agreement with the experimentally observed rigid, springy and snake-like orbit types [10].

The fiber model is applied to analyze the dynamics of both fully

flexible and rigid fibers in realistic flow fields. The diffusion of flexible fibers in a turbulent channel flow is shown to be governed by the flow fluctuations. The fully flexible and initially straight fibers evolve into coiled structures while being transported in the turbulent flow field. The reorientation of rigid fibers is analyzed in the turbulent flow of a conical diffuser. It is observed that the fiber reorientation occurs at the time-scale of the reciprocal average shear rate. Moreover, for both flexible and rigid fibers, the reorientation is dominated by fiber inertia, while the fiber length does not have any significant effect on the fiber reorientation.

The flexible fiber model is used to analyze the rheology of fiber suspensions. A novel method is proposed to compute the deviatoric stresses in suspensions with flexible and curved fibers. The effects of fiber flexibility and fiber curvature on the rheological properties of dilute suspensions are examined. The results show that the specific viscosity decreases and the first normal stress difference increases when the fiber flexibility increases. For large fiber bending ratios, the obtained results are in agreement with Batchelor's theoretical predictions for straight, rigid fibers [7]. For the curved, stiff fibers, the specific viscosity and the normal stress differences increase as the fiber curvature increases. The specific viscosity reaches its maximum value, and decreases when the fiber shape starts to become coiled. Similarly, the normal stress differences increase with the fiber curvature, and vanish when the symmetry of the fiber is restored. The observed relationship between the fiber properties and the rheology can be used to determine the mechanical properties of the fibers, which are not easily accessible by experiments. Fibers encountered in practical applications, including the mat-forming process, may have a wide range of fiber bending stiffness or equilibrium shapes. An accurate analysis of deformable and irregularly shaped fibers is thus of great practical importance.

The rigid fiber model is employed to study fiber aggregation in suspensions with rod-like fibers suspensions in turbulent flow of an asymmetric planar diffuser. The fibers are assumed to interact through short-range attractive forces in the dilute regime. The study shows that the darting fiber motion, triggered by the fiber inertia and the average flow gradients, leads to enhanced collisions between fibers, and to a significantly increased aggregation rate. To the author's knowledge, this mechanism of fiber aggregation has not been reported in the literature before.

Bibliography

[1] S. B. Lindström. *Modeling and simulation of paper structure development*. PhD thesis, Mid Sweden University, Sundsvall, Sweden, October 2008.

[2] A. Lundell, L. D. Söderberg, and P. H. Alfredsson. Fluid mechanics and papermaking. *Annu. Rev. Fluid Mech.*, 43:195–217, 2011.

[3] C. Ljus. *On Particle transport and turbulence modification in air-particle flows*. PhD thesis, Chalmers University of Technology, Göteborg, Sweden, 2000.

[4] G. B. Jeffery. The motion of ellipsoidal particles immersed in a viscous fluid. *Proc. Roy. Soc. London Ser. A*, 102:161–179, 1922.

[5] F. P. Bretherton. The motion of rigid particles in a shear flow at low reynolds number. *J. Fluid Mech.*, 14:284, 1962.

[6] R. G. Cox. The motion of long slender bodies in a viscous fluid. Part 2. Shear flow. *J. Fluid Mech.*, 45:625–657, 1971.

[7] G. K. Batchelor. The stress generated in a non-dilute suspension of elongated particels by pure straining motion. *J. Fluid Mech.*, 46:813–829, 1971.

[8] M. Rahnama, D. L. Koch, and E. S. G. Shaqfeh. The effects of hydrodynamic interactions on the orientation distribution in a fiber suspension subject to simple shear flow. *Phys. Fluids*, 7:487, 1995.

[9] E. Anczurowski and S. G. Mason. Particle motions in sheared suspensions. xxiv. rotation of rigid sheroids and cylinders. *Trans. Soc. Rheol.*, 12:209–215, 1968.

[10] O. L. Forgacs and S. G. Mason. Particle motions in sheared suspensions. X. Orbits of flexible threadlike particles. *J. Colloid. Sci.*, 14:473–491, 1959.

[11] E. Ganani and R. L. Powell. Suspensions of rodlike particles: Literature review and data correlations. *J. Compos. Mater.*, 19:194, 1985.

[12] C. A. Stover, D. L. Koch, and C. Cohen. Observations of fiber orientation in simple shear flow of semi-dilute suspensions. *J. Fluid Mech.*, 238:277–296, 1992.

[13] M. P. Petrich, D. L. Kohen, and C. Cohen. An experimental determination of the stress–microstructure relationship in semi-concentrated fiber suspensions. *J. Non-Newtonian Fluid Mech.*, 95:101–133, 2000.

[14] A. J. Pettersson, T. Wikström, and A. Rasmuson. Near wall studies of pulp suspension flow using LDA. *Can. J. Chem. Eng.*, 84:422–430, 2006.

[15] O. Melander and A. Rasmuson. PIV measurements of velocities and concentrations of wood fibers in pneumatic transport. *Exp. Fluids*, 37:293–300, 2004.

[16] J. Wu and C. K. Aidun. A numerical study of the effect of fibre stiffness on the rheology of sheared fiber suspensions. *J. Fluid Mech.*, 662:123–133, 2010.

[17] S. B. Lindström and T. Uesaka. A numerical investigation of the rheology of sheared fiber suspensions. *Phys. Fluids*, 21:083301, 2009.

[18] C. T. Crowe, M. Sommerfeld, and Y. Tsuji. *Multiphase Flows With Droplets and Particles*. CRC, New York, 1998.

[19] C. Ljus and A. E. Almstedt. Eulerian modelling of pulp-fibre transport in airflow. In *Two-Phase Flow Modelling and Experimentation*, Pisa, 1999.

[20] J. Hämäläinen, S. B. Lindström, T. Hämäläinen, and T. Niskanen. Papermaking fiber suspension flow simulations at multiple scales. *J. Eng. Math.*, 71(1):55–79, 2011.

[21] J. A. Olson, I. Frigaard, C. Chan, and J. P. Hämäläinen. Modeling a turbulent fibre suspension flowing in a planar contraction: The one-dimensional headbox. *Int. J. Multiphase Flow*, 30:51–66, 2004.

[22] P. J. Krochak, J. A. Olson, and D. M. Martinez. Fiber suspension flow in a tapered channel: The effect of flow/fiber coupling. *Int. J. Multiphase Flow*, 35:676–688, 2009.

[23] E. Svenning, A. Mark, F. Edelvik, E. Glatt, S. Rief, A. Wiegmann, L. Martinsson, R. Lai, M. Fredlund, and U. Nyman. Multiphase simulation of fiber suspension flows using immersed boundary methods. *Nordic Pulp Paper Res. J.*, 27(2):184–191, 2012.

[24] D. Qi. Direct simulations of flexible cylindrical fiber suspensions in finite Reynolds number flows. *J. Chem. Phys.*, 125:114901, 2006.

[25] C. F. Schmid, L. H. Switzer, and D. J. Klingenberg. Simulation of fiber flocculation: Effects of fiber properties and interfiber friction. *J. Rheol.*, 44:781–809, 2000.

[26] S. B. Lindström and T. Uesaka. Simulation of the motion of flexible fibers in viscous fluid flow. *Phys. Fluids*, 19:113307, 2007.

[27] L. H. Switzer and D. J. Klingenberg. Flocculation in simulations of sheared fiber suspensions. *Int. J. Multiphase Flow*, 30:67–87, 2004.

[28] T. Matsuoka and S. Yamamoto. Dynamic simulation of fiber suspensions in shear flow. *J. Chem. Phys.*, 102:2254–2260, 1995.

[29] O. L. Forgacs and S. G. Mason. Particle motions in sheared suspensions. IX. Spin and deformation of threadlike particles. *J. Colloid. Sci.*, 14:457–472, 1959.

[30] C. G. Joung, N. Phan-Thien, and X.J. Fan. Direct simulation of flexible fibers. *J. Non-Newtonian Fluid Mech.*, 99:1–36, 2001.

[31] C. G. Joung, N. Phan-Thien, and X.J. Fan. Viscosity of curved fibers in suspensions. *J. Non-Newtonian Fluid Mech.*, 102:1–17, 2002.

[32] R. F. Ross and D. J. Klingenberg. Dynamic simulation of flexible fibers composed of linked rigid bodies. *J. Chem. Phys.*, 106:2949–2960, 1997.

[33] S. B. Lindström and T. Uesaka. Simulations of semidilute suspensions of non-Brownian fibers in shear flow. *J. Chem. Phys.*, 128:024901, 2008.

[34] S. B. Lindström and T. Uesaka. Particle-level simulation of forming of the fiber network in papermaking. *Int. J. Eng. Sci.*, 46(9):858–876, 2008.

[35] S. B. Lindström, T. Uesaka, and U. Hirn. Evolution of the paper structure along the length of a twin-wire former. In S. J. l'Anson, editor, *14th Fund. Res. Symp.*, volume 1, pages 207–245. Oxford, UK, September 2009.

[36] H. G. Weller, G. Tabor, H. Jasak, and C.Fureby. A tensorial approach to computational continuum mechanics using object-oriented techniques. *Comp. Phys.*, 12(6):620–631, 1998.

[37] R. Pal. *Rheology of particulate dispersions and composites*, volume 136 of Surfactant Science Series. CRC Press, 1 edition, 2006.

[38] P. D. Clausen, S. G. Koh, and D. H. Wood. Measurements of a swirling turbulent boundary layer developing in a conical diffuser. *Exp. Therm. Fluid Sci.*, 6:39–48, 1993.

[39] C. U. Buice and J. K. Eaton. Experimental investigation of flow through an asymmetric plane diffuser. *J. Fluids Eng.*, 123:819–828, 2001.

[40] S. Obi, K. Aoki, and S. Masuda. Experimental and computational study of turbulent separating flow in an asymmetric plane diffuser. In *9th Symposium on Turbulent Shear Flows*, Koyoto, Japan, 16-19 August, 1993.

[41] A. D. Gosman and E. Ioannides. Aspects of computer simulation of liquid-fueled combustors. *J. Energy*, 7:482–490, 1983.